Simplified approach for quantitative calculations of optical pumping

Fred Atoneche, Anders Kastberg

EPJ manuscript No.
(will be inserted by the editor)

Simplified approach for quantitative calculations of optical pumping

Fred Atoneche[1] and Anders Kastberg[2]

[1] Laboratory of Research on Advanced Materials and Nonlinear Sciences, Department of Physics, Faculty of Science, University of Buea, P.O. Box 63, Buea, Cameroon, e-mail: fred.atoneche@ubuea.cm
[2] Université Côte dAzur, CNRS, Laboratoire de Physique de la Matière Condensée UMR 7336, Parc Valrose, 06100 Nice, France, e-mail: anders.kastberg@unice.fr

Received: date / Revised version: date

Abstract. We present a simple and pedagogical method for quickly calculating optical pumping processes based on linearised population rate equations. The method can easily be implemented on mathematical software run on modest personal computers, and can be generalized to any number of concrete situations. We also show that the method is still simple with realistic experimental complications taken into account, such as high level degeneracy, impure light polarization, and an added external magnetic field. The method and the associated mathematical toolbox should be of value in advanced physics teaching, and can also facilitate the preparation of research tasks.

PACS. 32.10.Fn Fine and hyperfine structure – 32.80.Xx Level crossing and optical pumping

1 Introduction

Preparation of the internal state of an atomic or molecular system by optical pumping was initially developed as a technique in the 1950's by Alfred Kastler [1,2], and the theoretical framework was well developed already in the 1970s (see *e.g.* [3,4]). Since then, optical pumping has been used in many different fields of fundamental and applied research. For example, optical pumping is important in fields like laser construction, precision spectroscopy, fundamental metrology, and medical imaging. Many concrete examples can be given.

Within the fields of laser cooling and trapping [5–8], and Bose-Einstein condensation [9,10], atomic orientation by optical pumping has played crucial roles, partly by providing routes for cooling mechanisms, and partly as a means for preparing a sample for optimum trapping. In quantum information, optical pumping provides a way to prepare a sample of, *e.g.*, cold atoms, thermal atoms, or ions embedded in a crystal, in particular states suitable for processing, or storage of the information. Similarly, for atomic clocks and frequency standards, an atomic system often needs to be prepared in a state that does not have a first-order Zeeman shift — a clock-state — with a high level of precision and reproducibility. In medical magnetic imaging, optical pumping of saturated alkali gases, combined with spin polarizing collisions with a biologically inactive gas, *e.g.* ^{129}Xe or ^{3}He, provides an alternative to traditional MRI imaging, avoiding ionizing radiation and a large apparatus (see, *e.g.*, [11–14]).

1.1 Optical pumping as a teaching tool

Optical pumping has proved to be a useful tool in physics teaching. There are articles on the didactics of the subject as early as 1960 [15]. The pedagogical usefulness is partly due to the fact that it is relatively easy to devise practicals where students get hands on experience on quantum physics, and partly due to the conceptual elegance and simplicity of the underlying theory.

Studies of optical pumping can facilitate the understanding of a great number of physical phenomena. This includes very fundamental concepts like electron spin and quantization axes, and ranges via atomic structure, the Zeeman effect and radiative transitions, to more applied subjects such as spectroscopy and magnetic resonance. The relative simplicity with which a student practical can be set up also provides excellent training in basic experimental physics, analysis of data, and specific techniques such as laser physics and optical manipulation and detection. Optical pumping is also a suitable problem for learning mathematical methods in physics, numerical calculations, and Monte-Carlo methods.

1.2 Quantifying optical pumping

When optical pumping is used as a technique, it is important to be able to optimize it, and to understand limitations in its efficiency due to, *e.g.*, reabsorption of scattered light, influence of ambient fields, collisional quenching, impure polarizations, or other types of perturbations. To achieve this, it is adamant to have models, as explicit as possible, where the optical pumping can be computed and optimized with relative ease. Ideally, these models should give quantitative results that are correct on an absolute scale, also for complex multi-level quantum systems, and for systems having unavoidable experimental limitations.

Many experiments that include optical pumping are of a probabilistic nature. This means that a sample has to be reset, and prepared in a given orientation periodically, often with a repetition rate as high as possible. Also, for some classes of experiments, there are severe constraints concerning the imperfection in the achieved atomic orientation. In these cases, it may be important to have an accessible tool to quantify the limitations as accurately as possible, in order to facilitate the optimization of the experiment.

In several practical applications, the optical pumping itself might have been quantifiable if it could have been studied in isolation. However, when it is just one component in a globally very complicated problem, it can be of great utility if the evolution of state populations, driven by optical pumping, can be reduced to explicit analytical expressions.

In student laboratories (as well as in research ones), a theoretical tool for quantitatively predicting the outcome of an optical pumping experiment can be applied in conjunction with experiments, in order to enhance learning and understanding, and the simpler this is — while still accurate — the better. Moreover, a comprehensive approximative model for the phenomenon can also be used as a practice ground for theoretical problem solving.

1.3 The goals of this work

With the above considerations in mind, we have developed a resource for optical pumping, that might be useful for researchers, educators and students alike. We present a simplified theoretical toolbox for making direct quantitative predictions of explicit optical pumping experiments. This includes real experimental complications such as high degrees of atomic state degeneracy, impurities in polarization, Zeeman shifts, and angular errors in the applications of magnetic fields and the designation of a quantization axis.

We are not investigating the interaction in its entirety. The aim is rather to find analytical expressions that have an optimum usefulness in terms of calculating produced atomic orientations, and which can be generally applied. We also want to provide methods that have a pedagogical value for physics students at various levels.

The method will here be presented by five concrete examples. In parallel, we publish program codes [16–20], long derived analytical expressions for some concrete situations, and also results for the latter [21–25]. This online publication will be gradually expanded to include increasingly more complex situations. Much more thorough and complete solutions to the atom-photon interaction have previously been published elsewhere (see, *e.g.* [26–29]). Another work that has similarities with our approach is [30].

2 Theory

Optical pumping can be applied between energy levels that are energetically distinct, or within a degenerate manifold. A limitation that we will adhere to in this paper is that the process will concern redistributions between quantum states that are stable, or have radiative lifetimes that are long compared to the time scales involved in the experiment considered.

One central ingredient in our simplified approach is to consider only the population in these (meta)stable states, and to ignore coherences. To justify this, we take the pumping light intensity to be below the one that would saturate the transition, which means that on average very few atoms will be in an excited state manifold. The rate of absorption is slow compared to the spontaneous emission, and the timescale for an absorption-emission cycle will be totally dominated by the slow absorption.

Mathematically, this means that we can (incoherently) couple ground state populations directly, with average rates determined by absorption rates and branching ratios. This way, we approximate the scattering processes with simple deterministic rate equations. That in turn gives a system of coupled equations greatly reduced from the complete formulation. The trade-off is that we lose all information of induced coherences and light shifts. The method will be strictly limited to the incoherent redistribution of population between ground state levels brought about by the absorption of a single resonant light field.

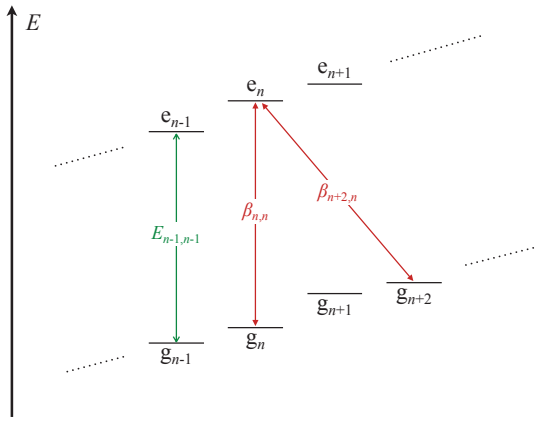

Fig. 1. Two sets of discrete atomic quantum states: one stable manifold labelled g_j, and another one consisting of levels with short radiative lifetimes, labelled e_k. The energy difference between each pair of one ground and one excited state is called $E_{jk} = \hbar\omega_{jk}$, exemplified by the green double arrow. The relative transition probabilities for the various transitions are called β_{jk}, exemplified by the red double arrows.

2.1 General

Consider a set of discrete atomic energy levels, as depicted in Fig. 1. We assume one set of 'ground state' levels, g_j. These are stable, or metastable, in the sense that their decay rate is very low compared to the relevant timescale for the experiment considered. The set of 'excited states', e_k, decay radiatively to the lower ensemble. Each of the two sets may be degenerate, almost degenerate or not degenerate at all.

We will assume one or several optical fields driving transitions between levels in the two manifolds. The frequencies of these will determine the number of levels to be considered, since very far detuned transitions can be neglected. We call the detunings of the transitions Δ_{jkm}, where the indices j and k are labels for the energy levels involved in the transition, and m is an index for the laser field (if more than one is applied). The relative transition strength (independent of intensity and detuning) for a transition is labelled β_{jk}. This is essentially the same as a square of a Clebsch-Gordan coefficient, but care has to be taken that these are normalized in a consistent way.

We call the time-dependent population in each of the ground levels G_n, and those in the excited levels Υ_n. This is normalized such that:

$$\sum_{j=1}^{N_\mathrm{g}} G_j + \sum_{k=1}^{N_\mathrm{e}} \Upsilon_k = 1\,, \tag{1}$$

where N_g and N_e are the total number of ground and excited states involved in the problem. If we call the transition probability between a pair of levels A_{jk}, and the radiative lifetime of the excited level τ_k, the natural linewidth of any transition from the excited level e_k will be:

$$\Gamma_k = \frac{1}{\tau_k} = \sum_{j=1}^{N_\mathrm{g}} A_{jk} = \Gamma_k \sum_{j=1}^{N_\mathrm{g}} \beta_{jk}\,. \tag{2}$$

Equation 2 provides a strict definition of the aforementioned relative transition rate, β_{jk}. It is the branching ratio of the radiative decay from level e_k to g_j (note that when we use a double index, we consistently write the index corresponding to the lower manifold first; and when we use a triple index, the third one refers to the driving field). With this definition, the normalization of the coefficients β_{jk} is:

$$\sum_{j}^{N_j} \beta_{jk} = 1\,. \tag{3}$$

The exact treatment of the problem would be to now write the atomic wave function as a superposition of all possible states and to then via the time dependent Schrödinger equation formulate the optical Bloch equation (see *e.g.* [31]). While that approach is exact, the size of the problem quickly becomes unmanageable when the system grows beyond a two-level atom. However, the approximation that we set all applied laser intensities to well below saturation means that we can set the probability amplitudes of all states in the excited manifold to be always close to zero. This is a grave simplification, since all coherences in the system are then discarded. Nevertheless, if we limit the study to

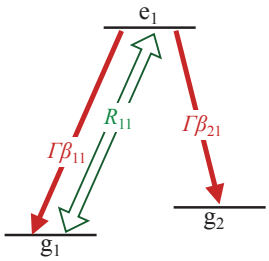

Fig. 2. A three-level system, driven from a ground state g_1, resulting in optical pumping of state g_2. The green double arrow represents the driving rate, R_{11}, and the red thick arrows represent spontaneous decay from the upper level, with the total rate $\Gamma_1 = \Gamma_1(\beta_{11} + \beta_{21})$.

the time evolutions of the ground state populations, and we stay well below saturation, the approximation will provide good answers to the specific question posed in this work.

Another way to state that driving fields are below saturation is that the intensity and detuning dependent absorption rates, $R_{jkl}(I, \Delta)$, are always slow compared to the decay rate of the excited states:

$$R_{jkl}(I.\Delta) = R_l(\Delta)\,\beta_{jk} \ll \Gamma_k\,. \tag{4}$$

$R_l(\Delta)$ is here the rate that corresponds to a pure two-level case (a Clebsch-Gordan coefficient of one). In the electric dipole approximation, with $I_{\rm sat}$ as the saturation intensity, the absorption rate is:

$$R_{jkl}(I.\Delta) = \beta_{jk}\,\frac{\Gamma_k}{2}\,\frac{(I/I_{\rm sat})}{1 + (I/I_{\rm sat}) + (2\Delta_{jkl}/\Gamma_k)^2}\,. \tag{5}$$

At the low intensities that we will consider, the power broadening term in the denominator can be omitted.

More accurately, we make the assumption that we will work in a regime where the scattering rate grows linearly with intensity. For intensities such that $I < I_{\rm sat}/5$, this should be a quite conservative approximation. If yet more accuracy is needed, the fraction in eq. 5 can be replaced by (for zero detuning):

$$\frac{(I/I_{\rm sat})}{1 + (I/I_{\rm sat})} \approx 1 - I/I_{\rm sat} + (I/I_{\rm sat})^2 - \ldots\,. \tag{6}$$

With higher intensity, there will be coherences and light shifts of the level, but as long as the only quantity searched for is the fractional populations of the lower levels, the method will give good results even for intensities that approach $I_{\rm sat}$.

2.1.1 Time evolution in the ground state manifold

We first consider a simplified example with a three-level system, as illustrated in Fig. 2. The transfer of the population from g_1 to g_2 is a two-step process: a driven excitation from g_1 to e_1, followed by spontaneous decay from e_1 to g_2. With the assumption that we drive far below saturation, the time scale for the total process will be dominated by the slow driving rate. The spontaneous decay will then essentially be instantaneous, on the time scale relevant for the experiment.

The state g_2 is not resonantly coupled to the laser field, and thus its population, $G_2(t)$, will increase with a rate that depends on the instantaneous population in e_1, $\Upsilon_1(t)$:

$$\frac{\rm d}{{\rm d}t}\,G_2(t) \approx \frac{G_2(t + {\rm d}t_\Gamma) - G_2(t)}{{\rm d}t_\Gamma} = \Upsilon_1(t)\,\Gamma_1\,\beta_{21}\,, \tag{7}$$

where ${\rm d}t_\Gamma \ll \Gamma_1^{-1}$ is an asymptotically short time interval. The population in e_1 in turn — which is always very low as long as $\Gamma_1 \gg R$ — will evolve as:

$$\frac{\rm d}{{\rm d}t}\,\Upsilon_1(t) \approx \frac{\Upsilon_1(t + {\rm d}t_R) - \Upsilon_1(t)}{{\rm d}t_R} = [G_1(t) - \Upsilon_1(t)]\;R_{11} - \Upsilon_1(t)\,\Gamma_1 \approx G_1(t)\,\beta_{11}\,R \approx \frac{\Upsilon_1(t + {\rm d}t_R)}{{\rm d}t_R}\,. \tag{8}$$

In this equation, the time interval ${\rm d}t_R \ll R^{-1}$ is also very brief, but it is long compared to the spontaneous decay: ${\rm d}t_R \gg {\rm d}t_\Gamma$. If we now look at the total process still in the short time interval ${\rm d}t = {\rm d}t_R + {\rm d}t_\Gamma \approx {\rm d}t_R$, the growth rate

of the population of g_2 will be the same as the instantaneous rate of increase of e_1, since we assume that subsequent radiative decay happens on a comparatively negligible time scale. We have:

$$\frac{\mathrm{d}}{\mathrm{d}t} G_2(t) \approx \frac{G_2(t+\mathrm{d}t) - G_2(t)}{\mathrm{d}t} \approx \frac{\Upsilon_1(t+\mathrm{d}t_R)}{\mathrm{d}t}\, \beta_{21} = G_1(t)\, \beta_{11}\beta_{12}\, R\,. \tag{9}$$

That is, the rate of optical pumping is entirely dominated by the scattering rate R, and it is weighted by the two involved coupling coefficients.

This can be generalized to the general system in Fig. 1, for which the equivalent analysis will yield:

$$\frac{\mathrm{d}}{\mathrm{d}t} G_n(t) = \sum_{j\neq n} G_j(t) \left[\sum_k R_{jk}\, \beta_{jk}\beta_{nk}\right] - G_n(t) \sum_k R_{nk}\, \beta_{nk}(1-\beta_{nk})\,. \tag{10}$$

The sum over j is over all ground state levels, and the sums over k goes over all excited levels. The first term is the replenishment of level gn from all other ground states, and the second term is the loss due to pumping out of the level. In most real cases, eq. 10 can be greatly simplified, since the sums rarely extend further than a few terms, as we shall see in the concrete examples in section 3.

2.2 Optical pumping in ^{87}Rb

The problem we have chosen to exemplify the method with is optical pumping within the ground state hyperfine structure (hfs) doublet of ^{87}Rb; 5s $^2S_{1/2}$ [32]. We assume narrowband optical pumping on the D2-line at $\lambda = 780$ nm. The upper state manifold is 5p $^2P_{3/2}$, and the pumping light is applied in order to achieve a certain desired distribution of the population of the ground states.

We derive explicit, analytical expressions for the time evolution of the level populations, as functions of interaction time, laser frequency, laser irradiance, and applied magnetic flux density. The method can readily be modified to other systems, and our derived equations are directly valid for other alkalis with the same nuclear spin as ^{87}Rb: $I = 3/2$, such as ^{7}Li, ^{23}Na, ^{39}K, and ^{41}K.

We break down this concrete example into schemes with either pure circular or linear polarization, and also a case with arbitrarily mixed polarization. In the case of circular polarization, the successive absorptions of photons carrying angular momenta, followed by spontaneous emission, will gradually align all atomic angular momenta with the propagation axis of the laser beam. In the case with linear polarization, the magnetic moment will become oriented in such a way that it gets a vanishing projection along a given direction, which makes it insensitive to first-order Zeeman shifts: a so called clock state. In one of the cases, both of the ground state levels will be coupled, which necessitates a second laser field (a *repumper*). We also include an example with an applied external magnetic field, which breaks the Zeeman degeneracy in both lower and upper levels.

2.2.1 The atom ^{87}Rb

A grotrian diagram showing the D2-transition in ^{87}Rb is presented in Fig. 3. The specific optical pumping configurations we study are:

1. Preparation of the stretched state $F_g = 2$, $M_g = +2$ by pumping on the transition $F_g = 2$ to $F_e = 3$: **Case 1**
2. Preparation of the clock state $F_g = 1$, $M_g = 0$ by pumping on the transition $F_g = 1$ to $F_e = 0$: **Case 2**
3. Preparation of the clock state $F_g = 2$, $M_g = 0$ by pumping on the transition $F_g = 2$ to $F_e = 2$: **Case 3**
4. Preparation of the stretched state $F_g = 2$, $M_g = +2$ by pumping on the transition $F_g = 2$ to $F_e = 3$, but with impure polarization: **Impure case**
5. Preparation of the stretched state $F_g = 2$, $M_g = +2$ by pumping on the transition $F_g = 2$ to $F_e = 3$, but with an added external magnetic field: **Zeeman case**

In the first two and the last two cases, it will suffice to include only one of the two hfs-ground states. In case 3, both hfs-states, and thus all 8 sub-states, have to be included.

2.2.2 Coupling coefficients

We need to know the transition probabilities (at resonance) for all involved transitions. Deriving these from the radiative lifetime of the upper levels, using a reduction of the electric dipole Hamiltonian is in principle straightforward. In this paper, we present the results of such a derivation, and we refer to textbooks such as [33] for a detailed description.

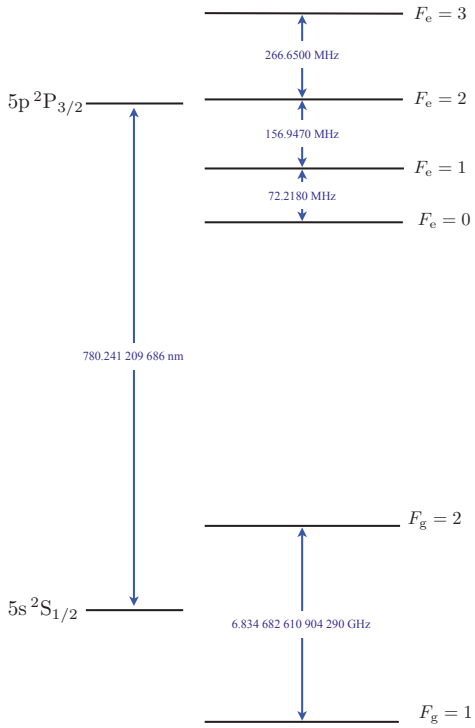

Fig. 3. Energy levels involved in the D2-transition in ^{87}Rb [32]. Each hfs-level has a degree of degeneracy of $2F + 1$. For this work, a subset (or the entirety) of the 8 Zeeman sub-levels in the $F_g = 2$ and $F_g = 1$ levels will constitute the manifold g_j, whereas a selection of the 16 excited states will be the excited manifold e_k.

We use a standard nomenclature for natural constants and atomic angular momentum quantum numbers, with $\gamma_{g/e}$ being a shorthand notation for the combination of electronic configurations (in the central-field approximation), and quantum numbers L and S the total atomic electronic orbital angular momentum and spin respectively. q is the polarization basis state.

The probability for spontaneous emission from any upper state, to a particular lower state is given by:

$$A(\gamma_e\, J_e I F_e M_e \to \gamma_g\, J_g I F_g M_g) = \Gamma_{x/y} = \beta_{x/y}\Gamma = (2F_e+1)(2J_g+1)\begin{Bmatrix} J_g & I & F_g \\ F_e & 1 & J_e \end{Bmatrix}^2 (2J_e+1)\begin{pmatrix} F_g & 1 & F_e \\ M_g & q & -M_e \end{pmatrix}^2 \Gamma\,. \quad (11)$$

The basis used for the polarization is with $q = 0$ corresponding to emission of light linearly polarized along $(\hat{z})$ – the quantization axis — ($\Delta M = 0$ transitions), and $q = \pm 1$ to light propagating along the $\hat{z}$-axis with clockwise/anti-clockwise circular polarization ($\Delta M = \pm 1$ transitions). With this convention, the relative strength of a cycling transition is unity. For the case of ^{87}Rb, the natural linewidth is $\Gamma_k = 2\pi \times 6.0666$ MHz.

3 Examples and results

3.1 Case 1

Here we assume light resonant with the transition $F_g = 2 \leftrightarrow F_e = 3$. We take the field as monochromatic and we assume that no other light is applied. The upper state $F_e = 3$ has no other decay channel than back to the $F_g = 2$ manifold; thus we can ignore all atoms in $F_g = 1$. Thereby, we have reduced the problem to one with 12 quantum states, instead of 24. The polarization of the exciting light is taken as purely σ^+. Thus, seen from the lower manifold, the only driven transitions are those with $\Delta M = +1$. In Fig. 4 we show this system, with the relative transition probabilities, β_{jk} — as computed with equation 11 — indicated. The transition probabilities that correspond to the driving transitions are indicated with full lines.

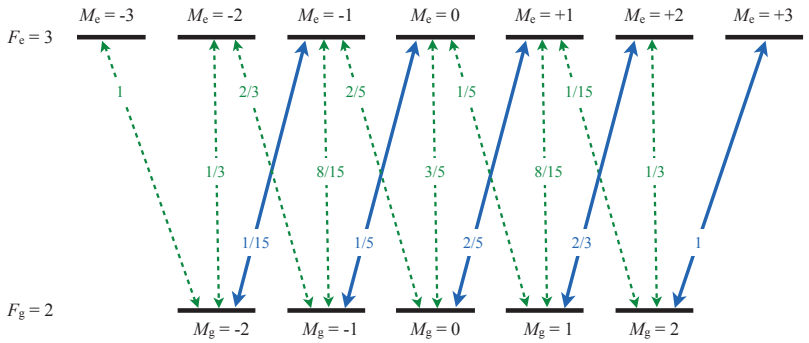

Fig. 4. Atomic states involved in the transition $F_g = 2 \leftrightarrow F_e = 3$ in the D2-line of ^{87}Rb, coupled by σ^+-light. The factors given on the transition arrows are the relative strengths of the transitions, given by eq. 11. Note that the sum of relative transition strengths from any upper state is unity. The transitions driven by circularly polarized light, σ^+, are indicated by full blue lines. The populations in the various states are labelled G_{-2}, Υ_{-3}, and so on.

Using the labels for the populations in the lower and upper manifolds that we introduced in the preceding section, we can write rate equations for the populations in the five subsystems G_j, as:

$$\begin{aligned}
\frac{\mathrm{d}}{\mathrm{d}t} G_{+2} &= \left[G_{+1}(t)\,\beta_{12}\beta_{22} + G_0(t)\,\beta_{01}\beta_{21}\right]\, R \\
\frac{\mathrm{d}}{\mathrm{d}t} G_{+1} &= \left[-G_{+1}(t)\,\beta_{12}\beta_{22} + G_0(t)\,\beta_{01}\beta_{11} + G_{-1}(t)\,\beta_{10}\beta_{10}\right]\, R \\
\frac{\mathrm{d}}{\mathrm{d}t} G_{0} &= \left[-G_0(t)\,\beta_{01}\,(\beta_{21}+\beta_{11}) + G_{-1}(t)\,\beta_{10}\beta_{00} + G_{-2}(t)\,\beta_{21}\beta_{01}\right]\, R \\
\frac{\mathrm{d}}{\mathrm{d}t} G_{-1} &= \left[-G_{-1}(t)\,\beta_{10}\,(\beta_{10}+\beta_{00}) + G_{-2}(t)\,\beta_{21}\beta_{11}\right]\, R \\
\frac{\mathrm{d}}{\mathrm{d}t} G_{-2} &= \left[-G_{-2}(t)\,\beta_{21}\,(\beta_{01}+\beta_{11})\right]\, R\,.
\end{aligned} \tag{12}$$

In deriving the eqs. 12, we have used the formalism developed in eq. 10. If the rates in eq. 12 are treated as those of components in a five-dimensional vector space, this can be written in vector notation as:

$$\frac{\mathrm{d}}{\mathrm{d}t}\boldsymbol{G}(t) = \begin{pmatrix}
0 & \beta_{12}\beta_{22} & \beta_{01}\beta_{21} & 0 & 0 \\
0 & -\beta_{12}\beta_{22} & \beta_{01}\beta_{11} & \beta_{10}\beta_{10} & 0 \\
0 & 0 & -\beta_{01}\,(\beta_{21}+\beta_{11}) & \beta_{10}\beta_{00} & \beta_{21}\beta_{01} \\
0 & 0 & 0 & -\beta_{10}\,(\beta_{10}+\beta_{00}) & \beta_{21}\beta_{11} \\
0 & 0 & 0 & 0 & -\beta_{21}\,(\beta_{01}+\beta_{11})
\end{pmatrix} R\,\boldsymbol{G}(t)\,. \tag{13}$$

Note that the spontaneous decay rate Γ does not appear explicitly (only as a parameter in R) in eq. 12 or eq. 13. This is a consequence of the assumption that the total rate of a transfer of one atom from one ground state to another one by optical pumping is completely dominated by the slower absorption rate.

Since the factors $\beta_{x/y}$ are known, the matrix can be written in explicit numerical form:

$$\frac{\mathrm{d}}{\mathrm{d}t}\boldsymbol{G}(t) = \frac{1}{225}\begin{pmatrix}
0 & 50 & 6 & 0 & 0 \\
0 & -50 & 48 & 9 & 0 \\
0 & 0 & -54 & 27 & 6 \\
0 & 0 & 0 & -36 & 8 \\
0 & 0 & 0 & 0 & -14
\end{pmatrix} R\,\boldsymbol{G}(t)\,. \tag{14}$$

This is easily solved analytically. Explicit equations are readily obtained for the time dependent state populations.

3.1.1 Results; case 1

An analytical solution to eq. 14 is straightforward. The last row in the matrix can be integrated directly, and when that is done, one can stepwise integrate all the others, from the bottom and up. The solutions (see also [16,21]) are

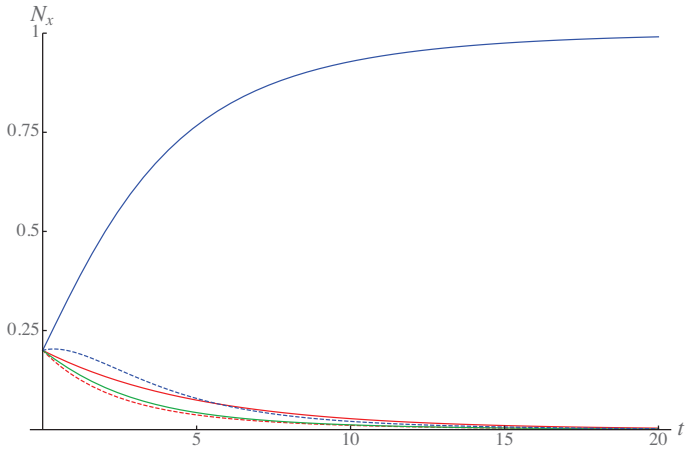

Fig. 5. Relative populations in the five sublevels, as functions of time in microseconds. This has been computed from eq. 15, corresponding to circular polarization and the transition $F_\mathrm{g} = 2 \leftrightarrow F_\mathrm{e} = 3$: full blue line G_{+2}, dashed blue line G_{+1}, full green line G_0, dashed red line G_{-1}, full red line G_{-2}.

shown in eq. 15, listed in the order that we have consistently used (inverse from the order of derivation).

$$
\begin{aligned}
G_{+2}(t) &= [G_{+2}(0) + G_{+1}(0) + G_0(0) + G_{-1}(0) + G_{-2}(0)] \\
&+ \left[-G_{+1}(0)\ \mathrm{e}^{\frac{4}{225}Rt} + G_0(0)\left(11 - 12\,\mathrm{e}^{\frac{4}{225}Rt}\right)\right. \\
&+ \frac{1}{14}\,G_{-1}(0)\left(-116\,\mathrm{e}^{\frac{2}{25}Rt} + 333\,\mathrm{e}^{\frac{4}{225}Rt} - 231\right) \\
&+ \left.\frac{1}{1540}\,G_{-2}(0)\left(2541 - 5060\,\mathrm{e}^{\frac{4}{225}Rt} + 4640\,\mathrm{e}^{\frac{2}{25}Rt} - 3661\,\mathrm{e}^{\frac{8}{45}Rt}\right)\right]\ \mathrm{e}^{-\frac{6}{25}Rt} \\
G_{+1}(t) &= \left[G_{+1}(0)\ \mathrm{e}^{\frac{4}{225}Rt} + 12G_0(0)\left(\mathrm{e}^{\frac{4}{225}Rt} - 1\right)\right. \\
&+ \frac{9}{14}\,G_{-1}(0)\left(28 - 37\,\mathrm{e}^{\frac{4}{225}Rt} + 9\,\mathrm{e}^{\frac{2}{25}Rt}\right) \\
&+ \left.\frac{1}{385}\,G_{-2}(0)\left(238\,\mathrm{e}^{\frac{8}{45}Rt} - 810\,\mathrm{e}^{\frac{2}{25}Rt} + 1265\,\mathrm{e}^{\frac{4}{225}Rt} - 693\right)\right]\ \mathrm{e}^{-\frac{6}{25}Rt} \\
G_0(t) &= \left[G_0(0) + \frac{3}{2}\,G_{-1}(0)\left(\mathrm{e}^{\frac{2}{25}Rt} - 1\right)\right. \\
&+ \left.\frac{1}{220}\,G_{-2}(0)\left(33 - 120\,\mathrm{e}^{\frac{2}{25}Rt} + 87\,\mathrm{e}^{\frac{8}{45}Rt}\right)\right]\ \mathrm{e}^{-\frac{6}{25}Rt} \\
G_{-1}(t) &= \left[G_{-1}(0) + \frac{4}{11}\,G_{-2}(0)\left(\mathrm{e}^{\frac{22}{225}Rt} - 1\right)\right]\ \mathrm{e}^{-\frac{4}{25}Rt} \\
G_{-2}(t) &= G_{-2}(0)\ \mathrm{e}^{-\frac{14}{225}Rt}\,.
\end{aligned}
\tag{15}
$$

In the limit of low saturation, and in keeping with the approximations made, eqs. 15 will be an excellent quantitative result for the populations of the Zeeman substates in the lower level, on an absolute scale.

Even though the expressions in eq. 15 are lengthy, they are explicit and they can easily be entered into any standard package for mathematics. An example of this is shown in [16]. Thus, for any set of parameters (starting values of the populations, intensity, and detuning) the time evolution of the populations can be easily computed quantitatively.

As an example, we assume the initial populations to be the same in all levels, and the total population normalized to unity ($G_{-2} = G_{-1} = G_0 = G_{+1} = G_{+2} = 0.2$). Furthermore, we set the intensity to a fifth of the saturation intensity ($I = I_\mathrm{sat}/5 \Rightarrow R \approx \Gamma/10$), and the detuning to zero. We then expect the population G_{+2} to grow monotonically towards unity, and all other levels to be eventually depleted. The result is shown in Fig. 5. We see that for this intensity, and exactly at resonance, the optical pumping time is of the order of 10 microseconds. We also see that the overall optical pumping time is limited by the small coupling coefficient governing the absorption from $M_\mathrm{g} = -2$, since this is last level to be emptied.

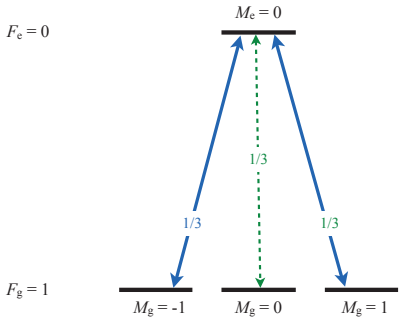

Fig. 6. Atomic states involved in the transition $F_g = 1 \leftrightarrow F_e = 0$, coupled by a combination of σ^+- and σ^--light. The factors given on the transition arrows are the relative strengths of the transitions, given by equation 11. The transitions driven by circularly polarised light are indicated by full red lines.

3.2 Case 2

In Case 2, we study the preparation of the clock state $F_g = 1$, $M_g = 0$, by pumping on the $F_g = 1 \leftrightarrow F_e = 0$ transition. The coupling light must be a combination of σ^+- and σ^--light. This system, with all its coupling coefficients, is depicted in Fig. 6, As for Case 1, the excited state — here $F_e = 0$ — only has one decay channel. Thus, also in this case, we only have to involve one of the ground state hfs-levels, this time $F_g = 1$.

We can immediately formulate the equations for the evolution of the ground state levels, following the same procedures as for case 1. If we assume that we have an equal distribution of intensities of σ^+- and σ^--light (this can easily be varied), the matrix form of the state populations evolution is:

$$\frac{\mathrm{d}}{\mathrm{d}t}\boldsymbol{G}(t) = \begin{pmatrix} -\beta_{10}\left(\beta_{00}+\beta_{10}\right) & 0 & \beta_{10}\beta_{10} \\ \beta_{10}\beta_{00} & 0 & \beta_{10}\beta_{00} \\ \beta_{10}\beta_{10} & 0 & -\beta_{10}\left(\beta_{00}+\beta_{10}\right) \end{pmatrix} R\,\boldsymbol{G}(t)\,, \tag{16}$$

and with numerical values for the coefficients, we get:

$$\frac{\mathrm{d}}{\mathrm{d}t}\boldsymbol{G}(t) = \frac{1}{18}\begin{pmatrix} -2 & 0 & 1 \\ 1 & 0 & 1 \\ 1 & 0 & -2 \end{pmatrix} R\,\boldsymbol{G}(t)\,. \tag{17}$$

3.2.1 Results; case 2

In this case, the analytical solution to eq. 17 is [17,22]:

$$\begin{aligned} G_{+1}(t) &= \frac{1}{2}\left[G_{-1}(0) - G_{+1}(0) + \left[G_{-1}(0) + G_{+1}(0)\right]\,\mathrm{e}^{\frac{1}{9}Rt}\right]\,\mathrm{e}^{-\frac{1}{6}Rt} \\ G_0(t) &= G_{-1}(0) + G_0(0) + G_{+1}(0) - \left[G_{-1}(0) + G_{+1}(0)\right]\,\mathrm{e}^{-\frac{1}{18}Rt} \\ G_{-1}(t) &= \frac{1}{2}\left[G_{+1}(0) - G_{-1}(0) + \left[G_{-1}(0) + G_{+1}(0)\right]\,\mathrm{e}^{\frac{1}{9}Rt}\right]\,\mathrm{e}^{-\frac{1}{6}Rt}\,. \end{aligned} \tag{18}$$

In Fig. 7, we show an example of optical pumping for this case. Here, we have assumed that the initial populations are 0.5 in the level M_g and 0.25 in the two others. Furthermore, we have set the intensity to a fifth of the saturation intensity ($I = I_{sat}/5 \Rightarrow R \approx \Gamma/10$), and the detuning to zero. We see that the clock state is optically pumped in a time scale of tens of microseconds.

3.3 Case 3

When we come to Case 3, we can no longer exclude one of the two ground-state hfs-levels. Linearly polarized light driving the $F_g = 2 \leftrightarrow F_e = 2$ transition will optically pump the state $F_g = 2$, $M_g = 0$, due to the electric dipole selection rule that the transition $M_g = 0 \leftrightarrow M_e = 0$ is forbidden when $F_g = F_e$. However, the states in $F_e = 2$ may also decay to $F_g = 1$. This can be counteracted by adding a *repumping laser*. This may be resonant from $F_g = 1$ to

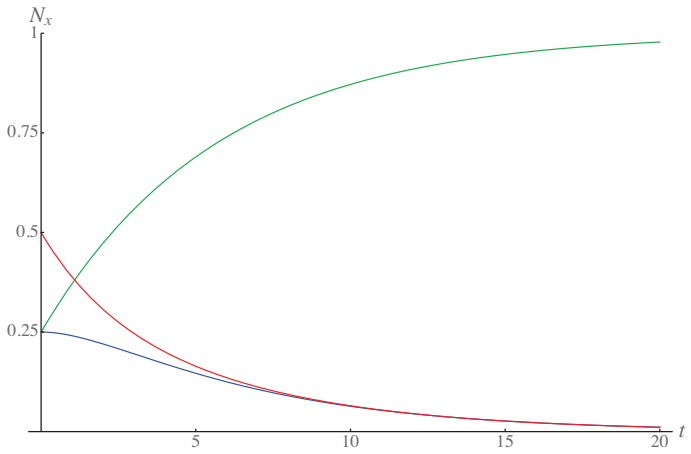

Fig. 7. Relative populations in the three sub-levels, as functions of time in microseconds, computed from Eq. 18. Full blue line G_1, full green line G_0, full red line G_{-1}.

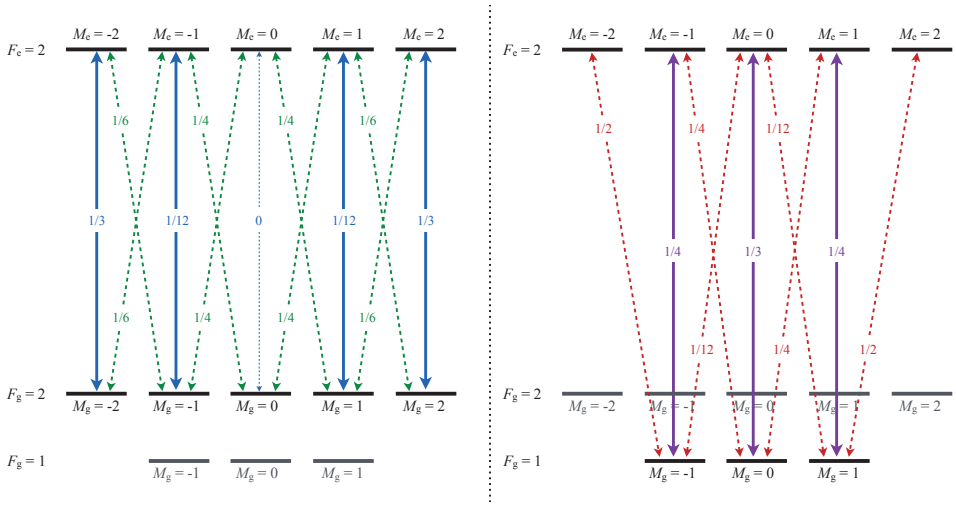

Fig. 8. Atomic states involved in the transitions $F_g = 2 \leftrightarrow F_e = 2$ and $F_g = 1 \leftrightarrow F_e = 2$, coupled by π-light. In the left panel, the factors given on the transition arrows are the relative strengths for $F_g = 2 \leftrightarrow F_e = 2$. In the right panel the relative strengths are those those for $F_g = 1 \leftrightarrow F_e = 2$. The transitions driven by linearly polarized light are indicated by full blue and violet lines respectively.

either $F_e = 1$ or $F_e = 2$. In order to limit the number of excited states in this study, we choose the latter of these options.

This problem is considerably more complex than Cases 1 and 2. We now have two driving fields and 13 involved atomic states. With our approximative method, where we only consider ground state levels, we will end up with an 8×8-matrix, but one that is still easy to solve exactly. In Fig. 8, we show a diagram of the involved atomic states, and the transition coefficients. The functional forms of the populations are:

$$
\begin{aligned}
\frac{\mathrm{d}}{\mathrm{d}t} G_{+2} &= \left[-G_{+2}(t)\,\beta_{22}\,(\beta_{12}+\alpha_{12}) + G_{+1}(t)\,\beta_{11}\beta_{21}\right]\,R_\beta + H_{+1}(t)\,\alpha_{11}\beta_{21}R_\alpha \\
\frac{\mathrm{d}}{\mathrm{d}t} G_{+1} &= \left[G_{+2}(t)\,\beta_{22}\beta_{12} - G_{+1}(t)\,\beta_{11}\,(\beta_{21}+\beta_{01}+\alpha_{11}+\alpha_{01})\right]\,R_\beta \\
&\quad + \left[H_{+1}(t)\,\alpha_{11}\beta_{11} + H_0(t)\,\alpha_{00}\beta_{10}\right]\,R_\alpha \\
\frac{\mathrm{d}}{\mathrm{d}t} G_{0} &= \left[G_{+1}(t)\,\beta_{11}\beta_{01} + G_{-1}(t)\,\beta_{11}\beta_{01}\right]\,R_\beta + \left[H_{+1}(t)\,\alpha_{11}\beta_{01} + H_{-1}(t)\,\alpha_{11}\beta_{01}\right]\,R_\alpha \\
\frac{\mathrm{d}}{\mathrm{d}t} G_{-1} &= \left[-G_{-1}(t)\,\beta_{11}\,(\beta_{21}+\beta_{01}+\alpha_{11}+\alpha_{01}) + G_{-2}(t)\,\beta_{22}\beta_{12}\right]\,R_\beta \\
&\quad + \left[H_0(t)\,\alpha_{00}\beta_{10} + H_{-1}(t)\,\alpha_{11}\beta_{11}\right]\,R_\alpha \\
\frac{\mathrm{d}}{\mathrm{d}t} G_{-2} &= \left[G_{-1}(t)\,\beta_{11}\beta_{21} - G_{-2}(t)\,\beta_{22}\,(\beta_{12}+\alpha_{12})\right]\,R_\beta + H_{-1}(t)\,\alpha_{11}\beta_{21}R_\alpha \\
\frac{\mathrm{d}}{\mathrm{d}t} H_{+1} &= \left[G_{+2}(t)\,\beta_{22}\alpha_{12} + G_{+1}(t)\,\beta_{11}\alpha_{11}\right]\,R_\beta \\
&\quad + \left[-H_{+1}(t)\,\alpha_{11}\,(\beta_{21}+\beta_{11}+\beta_{01}+\alpha_{01}) + H_0(t)\,\alpha_{00}\alpha_{10}\right]\,R_\alpha \\
\frac{\mathrm{d}}{\mathrm{d}t} H_{0} &= \left[G_{+1}(t)\,\beta_{11}\alpha_{01} + G_{-1}(t)\,\beta_{11}\alpha_{01}\right]R_\beta \\
&\quad + \left[H_{+1}(t)\,\alpha_{11}\alpha_{01} - H_0(t)\,\alpha_{00}\,(\beta_{10}+\beta_{10}+\alpha_{10}+\alpha_{10}) + H_{-1}(t)\,\alpha_{11}\alpha_{01}\right]\,R_\alpha \\
\frac{\mathrm{d}}{\mathrm{d}t} H_{-1} &= \left[G_{-1}(t)\,\beta_{11}\alpha_{11} + G_{-2}(t)\,\beta_{22}\alpha_{12}\right\}\,R_\beta \\
&\quad + \left[H_0(t)\,\alpha_{00}\alpha_{10} - H_{-1}(t)\,\alpha_{11}\,(\beta_{21}+\beta_{11}+\beta_{01}+\alpha_{01})\right\}\,R_\alpha
\end{aligned}
\quad . \tag{19}
$$

Here, we have retained $G_{+2}(t)$, β_{22}, etc., as notation for the level population and transition coefficients related to $F_\mathrm{g} = 2$. For $F_\mathrm{g} = 1$, we introduce the symbols $H_{+1}(t)$ and α_{12}, etc.. In numerical form, the matrix becomes:

$$
\frac{\mathrm{d}}{\mathrm{d}t}\boldsymbol{G}(t) = \frac{1}{144}
\begin{pmatrix}
-32\,R_2 & 2\,R_2 & 0 & 0 & 0 & 6\,R_1 & 0 & 0 \\
8\,R_2 & -11\,R_2 & 0 & 0 & 0 & 3\,R_1 & 12\,R_1 & 0 \\
0 & 3\,R_2 & 0 & 3\,R_2 & 0 & 9\,R_1 & 0 & 9\,R_1 \\
0 & 0 & 0 & -11\,R_2 & 8\,R_2 & 0 & 12\,R_1 & 3\,R_1 \\
0 & 0 & 0 & 2\,R_2 & -32\,R_2 & 0 & 0 & 6\,R_1 \\
24\,R_2 & 3\,R_2 & 0 & 0 & 0 & -27\,R_1 & 4\,R_1 & 0 \\
0 & 3\,R_2 & 0 & 3\,R_2 & 0 & 9\,R_1 & -32\,R_1 & 9\,R_1 \\
0 & 0 & 0 & 3\,R_2 & 24\,R_2 & 0 & 4\,R_1 & -27\,R_1
\end{pmatrix}
\boldsymbol{G}(t)\,. \tag{20}
$$

with rows and columns ordered as the equations in eq. 19.

3.3.1 Results; case 3

Also in this case, it is readily possible to derive explicit analytical expressions for the population. However, they become very lengthy, and are not suitable for display. If faster convergence is desired, parameter values can be set before the solution of eq. 20, and level populations as function of time can be found very quickly.

Fig. 9, is an example of the calculated time evolution of the eight ground state levels [18,23]. In this example, we have taken the initial populations in the five levels of the $F_\mathrm{g} = 2$ hyperfine structure level of the ground state as $G_{2,+2} = G_{2,+1} = 0.2$, $G_{2,0} = 0$, and $G_{2,-1} = G_{2,-2} = 0.1$; and those in $F_\mathrm{g} = 1$ as $G_{1,+1} = 0.2$, and $G_{1,0} = G_{1,-1} = 0.1$. Furthermore, we have set the intensity of linearly polarized light for the $F_\mathrm{g} = 2 \leftrightarrow F_\mathrm{e} = 2$ to a fifth of the saturation intensity ($I = I_\mathrm{sat}/5 \Rightarrow R \approx \Gamma/10$) while the light intensity for the repumping transition is set to one tenth of the saturation intensity. The detuning for both transitions is set to zero. The result is again the expected; the population of the optically pumped clock state, $G_{2,0}$, grows monotonically towards 1, as all other levels are depleted.

3.4 Impure polarisation

In any real experiment, there is always a finite impurity in the light polarization. This comes about due to, for example, imperfect polarization components, birefringence in windows and other optics, or an uncertainty in the determination of the quantization axis. When a pure state is crucial for an experiment, the imperfect optical pumping that follows from this imperfect polarization may have important detrimental effects. Therefore being able to quantify the effects

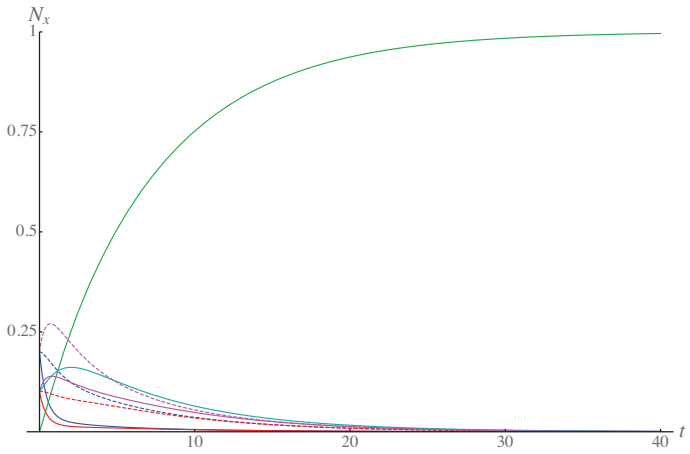

Fig. 9. Relative populations in all eight sub-levels, as functions of time in microseconds. This has been computed by a solution of Eq. 20. Full blue line $F_g = 2$, $M_g = +2$; dashed blue line $F_g = 2$, $M_g = +1$; full green line $F_g = 2$, $M_g = 0$; dashed red line $F_g = 2$, $M_g = -1$; full red line $F_g = 2$, $M_g = 12$; full magenta line $F_g = 1$, $M_g = +1$; full cyan line $F_g = 1$, $M_g = 0$; dashed magenta line $F_g = 1$, $M_g = -1$.

of an impure polarization on the level population is important. To illustrate how well our method works also for cases with impure polarization, we take the Case 1 from above as an example, and assume that the exciting light is not 100% polarized as σ^+.

Any light field, with total intensity I, exciting an atom can always be decomposed into the intensity components σ^+, π, and σ^- as:

$$\begin{aligned} I_{\sigma^+} &= c_+ I \\ I_{\pi} &= c_\pi I \\ I_{\sigma^-} &= c_- I \,. \end{aligned} \tag{21}$$

With several light fields with different polarizations present, different ground states can be coherently coupled through interaction with two light fields. However, in this study, we will ignore this effect. This is not a serious limitation for two reasons: we restrict the study to unsaturated transitions and we focus on level populations only.

For each of these polarization components, there will be a correspondinghttps://preview.overleaf.com/public/xksknsthbdjc/in evolution matrix. We call these M_{σ^+}, M_π and M_{σ^-}. M_{σ^+} will be the matrix given in eq. 14, and M_{σ^-} will be its counterpart for opposite polarization (the orders of both rows and columns have to be reversed). The remaining matrix is easily obtained from the coefficients in Fig. 4:

$$M_\pi = \frac{1}{225} \begin{pmatrix} -50 & 8 & 0 & 0 & 0 \\ 50 & -56 & 27 & 0 & 0 \\ 0 & 48 & -54 & 48 & 0 \\ 0 & 0 & 27 & -56 & 50 \\ 0 & 0 & 0 & 8 & -50 \end{pmatrix} . \tag{22}$$

The evolution of the population is then calculated by solving the equation:

$$\frac{\mathrm{d}}{\mathrm{d}t} \boldsymbol{G}(t) = MR\,\boldsymbol{G}(t) = (c_+ M_{\sigma^+} + c_\pi M_\pi + c_- M_{\sigma^-})\, R\,\boldsymbol{G}(t) \,. \tag{23}$$

3.4.1 Results; impure case

Equation 23 can be solved and analytical results as functions of the intensity distribution can be derived [19,24]. In figure 10, we show an example of an evolution of the populations of the five involved levels, based on the solution of the evolution equation (eq. 23), with the relative intensities set to $c_\pi = 0.025$, $c_+ = 0.95$ and $c_- = 0.025$. In this example, we have assumed that the initial populations are the same in all five levels, and that the total population normalized to unity ($G_{-2} = G_{-1} = G_0 = G_{+1} = G_{+2} = 0.2$). Furthermore, we set the intensity to a fifth of the saturation intensity ($I = I_{\mathrm{sat}}/5 \Rightarrow R \approx \Gamma/10$), and the detuning to zero.

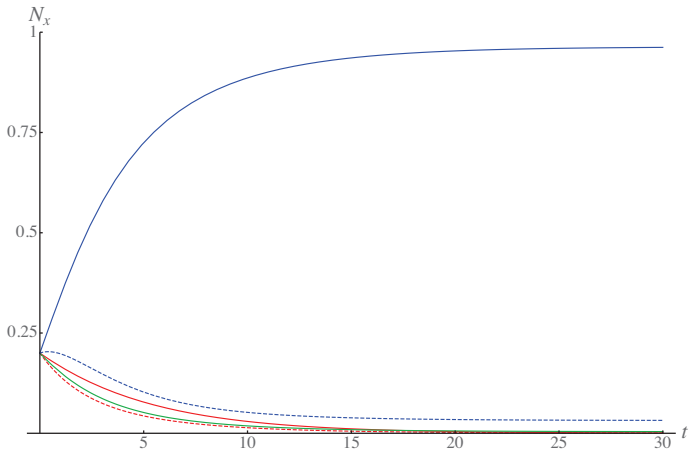

Fig. 10. Relative populations in the five sub-levels, as functions of time in microseconds. This has been computed by a solution of Eq. 23. Full blue line G_{+2}, dashed blue line G_{+1}, full green line G_0, dashed red line G_{-1}, full red line G_{-2}.

The population of the optically pumped level, G_{+2}, grows monotonically towards 1, as all other levels are gradually depleted. For these particular parameters, the asymptotic values of the populations are:

$$\begin{aligned} G_{-2}(t \to \infty) &= 0.000083 \\ G_{-1}(t \to \infty) &= 0.00042 \\ G_0(t \to \infty) &= 0.0040 \\ G_{+1}(t \to \infty) &= 0.032 \\ G_{+2}(t \to \infty) &= 0.96\,. \end{aligned} \tag{24}$$

3.5 The Zeeman shifted case

It is common to superimpose a homogeneous, static magnetic field on a sample that is to be optically pumped. This will then determine the quantization axis, and as long as the field is stronger than any stray fields, uncontrolled Larmor precession can be avoided.

There will always be a finite uncertainty in how well the polarization and the wave vector will be commensurate with the magnetic field direction. Such errors can be quantified following the procedure in the preceding section. With our method it is also easy to incorporate in the calculation the changes to the optical pumping rates due to the finite magnetic field and its associated Zeeman shift.

For simplicity, we will again take Case 1 as an example, and we will assume that the propagation direction of the circularly polarized light is perfectly parallel with the magnetic field. A direct consequence of the external field is that the five sub-levels will no longer be degenerate. The state dependent Zeeman shifts will in turn make the detunings $\Delta_{x/y}$ different for all transitions, and thus also the rates $R^{(x,y)}$ will be unequal (the indices x and y here refer respectively to the lower and upper states involved in a driven transition).

We limit this example to a case with relatively weak magnetic fields, where Paschen-Back effects do not have to be taken into account (for ^{87}Rb, this means that the field cannot be much stronger than 0.005 T.). In this case, the Zeeman shifts are:

$$\begin{aligned} E_{\mathrm{Z}} &= g_F\, M_F\, \mu_{\mathrm{B}} B\,, \\ g_F &= g_J\, \frac{F(F+1) - I(I+1) + J(J+1)}{2\,F(F+1)}\,. \end{aligned} \tag{25}$$

Here, B is the amplitude of the magnetic flux density, and g_J and g_F are the gyromagnetic ratios for the fine structure and hyperfine structure, respectively.

In the case of ^{87}Rb, we have $g_J = 2.00233113$ for 5s $^2\mathrm{S}_{1/2}$, and $g_J = 1.3362$ for 5p $^2\mathrm{P}_{3/2}$ [32]. For the hfs-levels involved, this in turn means that $g_F = 0.500583 \approx 1/2$ for $F_{\mathrm{g}} = 2$ in the ground state, and $g_F = 0.6681 \approx 2/3$ for $F_{\mathrm{e}} = 3$ in the excited state. The Zeeman shifted detunings then become:

$$\Delta_{x/y} = \omega - \left(\omega_0 + \frac{E_{\mathrm{Z}y} - E_{\mathrm{Z}x}}{\hbar}\right) \tag{26}$$

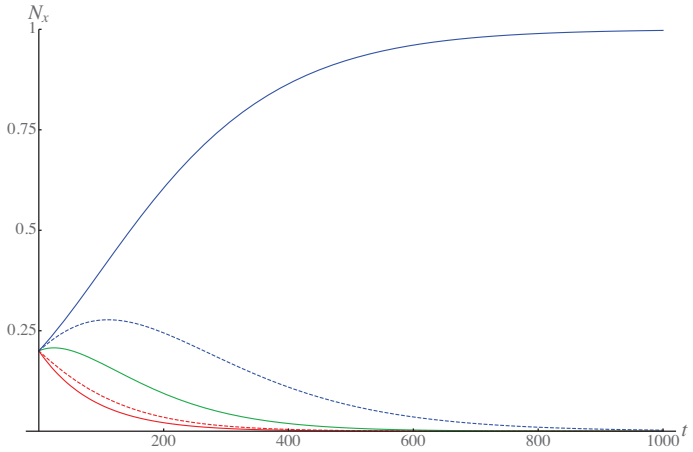

Fig. 11. Relative populations in the five sub-levels, as functions of time in microseconds, for the laser frequency $\omega = \omega_0$. This has been computed by a solution of Eq. 27. Full blue line G_{+2}, dashed blue line G_{+1}, full green line G_0, dashed red line G_{-1}, full red line G_{-2}.

In this equation, E_{Zx} and E_{Zy} are the energy Zeeman shifts in the lower and upper states respectively, ω_0 is the resonance angular frequency for $B = 0$, and ω is the angular frequency of the monochromatic light field. Generalizing the derivation made for Case 1, for the case with Zeeman shifted levels, then means that the matrix in equation 14 changes to:

$$\frac{\mathrm{d}}{\mathrm{d}t}\boldsymbol{G}(t) = \frac{1}{225}\begin{pmatrix} 0 & 25\,R^{(+1,+2)} & 6\,R^{(0,+1)} & 0 & 0 \\ 0 & -25\,R^{(+1,+2)} & 48\,R^{(0,+1)} & 9\,R^{(-1,0)} & 0 \\ 0 & 0 & -54\,R^{(0,+1)} & 27\,R^{(-1,0)} & 6\,R^{(-2,-1)} \\ 0 & 0 & 0 & -36\,R^{(-1,0)} & 8\,R^{(-2,-1)} \\ 0 & 0 & 0 & 0 & -14\,R^{(-2,-1)} \end{pmatrix}\boldsymbol{G}(t)\,. \tag{27}$$

Also this can be solved to yield analytical expressions for the populations, now also as functions of B.

3.5.1 Results; Zeeman case

With two independent variables, time and laser frequency, the solution becomes a bit more demanding computationally, in particular if the magnetic field is left as a selectable parameter. However, with modern computing facilities, this is still a modest problem. With a limited desktop computing program, a faster way to solve eq. 27 is to preselect the magnetic field and to then solve the equation numerically [20,25].

In Fig. 11, we show an example of an evolution of the populations of the involved levels for the laser frequency $\omega = \omega_0$ (corresponding to zero detuning for all transitions in the limit of zero field). Here we have assumed that the initial populations are the same in all five levels, and we have set the intensity to a tenth of the saturation intensity ($I = I_{\mathrm{sat}}/10$), and the magnetic field intensity to 0.002 T. The population of the optically pumped level, G_{+2}, grows monotonically towards 1, as all other levels are depleted. Note that the growth of the population of level G_{+2} towards one is slower than that in case 1, where there was no external magnetic field.

The same results as those in Fig. 11 can also be displayed as function of frequency, for a given time. This is shown in fig. 12. Yet another way to illustrate the optical pumping in this case is in a surface diagram, as function of both time and detuning. This is done in Fig. 13 for the optically pumped stretched state.

4 Discussion and conclusions

We have presented a method which facilitates quickly quantify optical pumping in a laboratory. In the limit of low saturation and slow absorption rates, exact analytical expressions for populations of the ground state are obtained. The objective with the method we present is to provide a *simple and fast* way to calculate optical pumping phenomena quantitatively. This should be a resource for an experimentalist when designing, or assessing, an experiment in for example quantum information, atomic frequency standards, magnetic imaging with polarised gases, or any other field where optical pumping may play a crucial role. With our introduced simplifications, it is straightforward to quantify the adverse effects on optical pumping by, *e.g.*, an impure polarization, or other experimental artefacts.

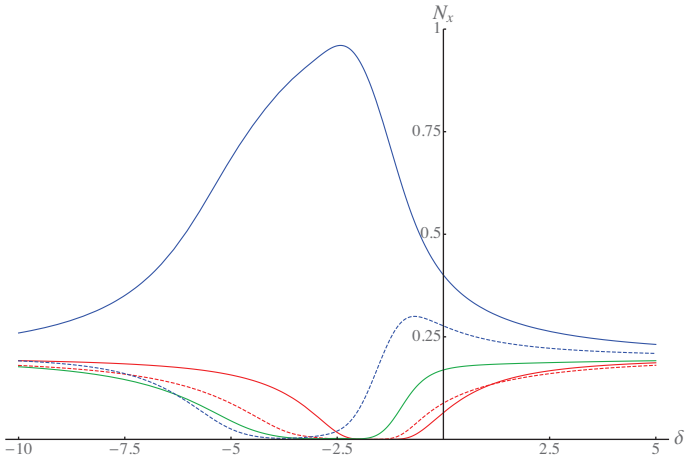

Fig. 12. Relative populations in the five sub-levels, as functions of detuning in units of the natural linewidth, Γ, for the optical pumping time $t = 100$ μs. This has been computed by a solution of Eq. 27. Full blue line G_{+2}, dashed blue line G_{+1}, full green line G_0, dashed red line G_{-1}, full red line G_{-2}.

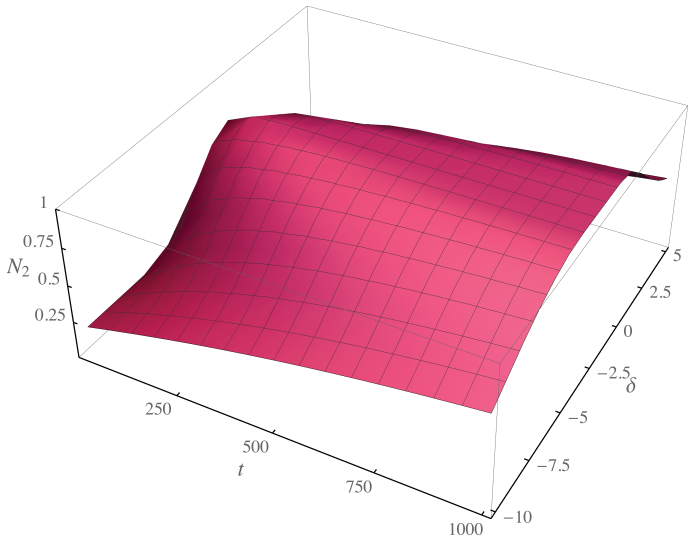

Fig. 13. Relative populations in sub-levels $M_g = +2$, as function of detuning in units of the natural linewidth, Γ, and time in units of microseconds.

The simplicity of our model also opens up the possibility for various other extensions. For example, in an optically dense sample, frequently necessary in quantum information applications, the maximum achievable optical pumping will be limited by re-scattering. This should be possible to include in the model, and a study of this effect will follow in a future work. The case for magnetic imaging usually involves very dense gases and strongly collisional broadening. There, limitations come from the complicated process of spin-exchanging collisions. Also analyses of that could potentially be facilitated if the included optical pumping problem is reduced to directly computable explicit expressions. Moreover, the inhomogeneous linewidth in the sample, and the finite bandwidth of the exciting light can be added to the analysis.

We believe that our resource could serve as a useful tool in physics teaching. Based on our methods, students could readily compute optical pumping rates for a number of different physical systems, and thereby gain insight in how to apply the included atomic physics properly, and how to use different computational tools. There are ample possibilities to combine this with laboratory practicals — either ones preprepared by teachers, or ones designed by students themselves. While doing this, performing simple and quick calculations on the side will provide insight in the importance in experimental imperfections in parameters such as, for example, polarization impurity.

In this article, we provide but a few examples of optical pumping problems. All these examples, with detailed solutions, and numerical code for the solution can be found in [16–25]. Adjacent to those files, there are also other examples, and this resource will be progressively updated with further examples.

References

1. A. Kastler, J. Phys. Radium **11**, 255 (1950)
2. A. Kastler, J. Opt. Soc. Am. **47**, 460 (1957)
3. R. Bernheim, Am. J. Phys. **35**, 167 (1967)
4. W. Happer, Rev. Mod. Phys. **44**, 169 (1972)
5. S. Chu, Rev. Mod. Phys. **70**, 685 (1998)
6. C. Cohen-Tannoudji, Rev. Mod. Phys. **70**, 707 (1998)
7. W.D. Phillips, Rev. Mod. Phys. **70**, 721 (1998)
8. L. Fallani, A. Kastberg, EPL **110**, 53001 (2015)
9. E.A. Cornell, C.E. Wieman, Rev. Mod. Phys. **74**, 875 (2002)
10. W. Ketterle, Rev. Mod. Phys. **74**, 1131 (2002)
11. T.G. Walker, W. Happer, Rev. Mod. Phys. **69**, 629 (1997)
12. I. Ruset, S. Ketel, F. Hersman, Phys. Rev. Lett. **96**, 053002 (2006)
13. T.G. Walker, J. Phys: Conference Series **294**, 012001 (2011)
14. D.M.L. Lilburn, G.E. Pavlovskaya, T. Meersmann, Journal of magnetic resonance **229**, 173 (2013)
15. R.L. de Zafra, Am. J. Phys. **28**, 646 (1960)
16. F. Atoneche, A. Kastberg, figshare (2016), https://dx.doi.org/10.6084/m9.figshare.3750531
17. F. Atoneche, A. Kastberg, figshare (2016), https://dx.doi.org/10.6084/m9.figshare.3750549.v1
18. F. Atoneche, A. Kastberg, figshare (2016), https://dx.doi.org/10.6084/m9.figshare.3756612
19. F. Atoneche, A. Kastberg, figshare (2016), https://dx.doi.org/10.6084/m9.figshare.3858918
20. F. Atoneche, A. Kastberg, figshare (2016), https://dx.doi.org/10.6084/m9.figshare.3978684
21. F. Atoneche, A. Kastberg, figshare (2016), https://dx.doi.org/10.6084/m9.figshare.3397681
22. F. Atoneche, A. Kastberg, figshare (2016), https://dx.doi.org/10.6084/m9.figshare.3750702
23. F. Atoneche, A. Kastberg, figshare (2016), https://dx.doi.org/10.6084/m9.figshare.3756801
24. F. Atoneche, A. Kastberg, figshare (2016), https://dx.doi.org/10.6084/m9.figshare.3859260
25. F. Atoneche, A. Kastberg, figshare (2016), https://dx.doi.org/10.6084/m9.figshare.3979227
26. A. Taichenachev, A. Tumaikin, V. Yudin, G. Nienhuis, Phys. Rev. A **69**, 033410 (2004)
27. B. Gao, Phys. Rev. A **48**, 2443 (1993)
28. B. Gao, Phys. Rev. A **49**, 3391 (1994)
29. B. Gao, Phys. Rev. A **50**, 4139 (1994)
30. J. Sagle, R.K. Namiotka, J. Huennekens, J. Phys. B: At. Mol. Opt. Phys. **29**, 2629 (1996)
31. R. Loudon, *Quantum theory of light*, 3rd edn. (Oxford Science Publications, Oxford, 2000)
32. D.A. Steck, *Rubidium 87 D Line Data* (2001), `http://steck.us/alkalidata/rubidium87numbers.pdf`
33. R.D. Cowan, *The theory of atomic structure and spectra* (University of California press, Berkeley, 1981)